Supercritical fluid extraction of essential oil from chamomile flowers: modelling, and parameter estimation

Oliwer Sliczniuk[a,*], Pekka Oinas[a]

[a]Aalto University, School of Chemical Engineering, Espoo, 02150, Finland

ARTICLE INFO

Keywords:
Supercritical extraction
Parameter estimation
Mathematical modelling

ABSTRACT

This study investigates the supercritical extraction process of essential oil from chamomile flowers. Essential oils of chamomile are used extensively for medicinal purposes. Many different products of chamomile have been developed, the most popular of which is in the form of herbal tea. A distributed-parameter model describes the fluid-solid extraction process. The concept of quasi-one-dimensional flow is applied to reduce the number of spatial dimensions. The flow is assumed to be uniform across any cross-section, although the area available for the fluid phase can vary along the extractor. The physical properties of the solvent are estimated from the Peng-Robinson equation of state. Model parameters, including the partition factor, internal diffusion coefficient, axial diffusion coefficient, and decaying factor, were determined through maximum likelihood estimation based on experimental data, with the assumption of normally distributed errors. A set of laboratory experiments was performed under multiple constant operating conditions: $30 - 40°C$, $100 - 200$ bar, and $3.33 - 6.67 \times 10^{-5}$ kg/s.

1. Introduction

This study investigates the extraction of essential oil from chamomile flowers (Matricaria chamomilla L.) via supercritical fluid extraction techniques and the modelling of this process. Chamomile is a medicinal herb widely cultivated in southern and eastern Europe—such as Germany, Hungary, France, and Russia. It can be found outside of Europe in Brazil as discussed by Singh et al. [1]. This plant is distinguished by its hollow, bright gold cones, housing disc or tubular florets and surrounded by about fifteen white ray or ligulate florets. Chamomile has been used for its medicinal benefits, serving as an anti-inflammatory, antioxidant, mild astringent, and healing remedy. Chamomile's aqueous extract is widely used to calm nerves and mitigate anxiety, hysteria, nightmares, insomnia, and other sleep-related conditions, according to Srivastava [2]. Orav et al. [3] reported that oil yields from dried chamomile samples ranged from 0.7 to 6.7 mL/kg. The highest yields of essential oil, between 6.1 and 6.7 mL/kg, were derived from chamomile sourced from Latvia and Ukraine, while chamomile from Armenia exhibited a lower oil content of 0.7 mL/kg.

Evaluating the economic viability of the process is essential when choosing the suitable technology for essential oil extraction. Traditional methods, such as distillation and organic solvent extraction, are commonly employed but come with drawbacks. Distillation, for example, involves high temperatures that can lead to the thermal degradation of heat-sensitive compounds. This limitation has led to the increased popularity of alternative techniques like supercritical fluid extraction. Supercritical carbon dioxide is appealing due to its distinctive properties: it is inflammable, non-toxic, and is non-corrosive. CO_2 is the most used supercritical fluid, sometimes modified by co-solvents such as ethanol. Supercritical fluids are capable of exhibiting both gas- and liquid-like properties, allowing for adjustable dissolving power through changes in operating conditions.

The literature offers various mathematical models to describe the extraction of valuable compounds from a biomass. Selecting a model requires a deep understanding of the physical processes, as each model is built on specific assumptions, mass transfer mechanisms and equilibrium dynamics.

The model proposed by Reverchon et al. [4] is the hot ball model, which is based on an analogy to heat transfer and describes an extraction process from solid particles. The model is based on assumptions that that particles contains low quantities of solute and solubility is not a limiting factor.

The Broken-and-Intact Cell model, proposed by Sovova [5], assumes that external surfaces of particles are mechanically disrupted, allowing the solvent's access to the solute in broken cells, while the solute in intact cells remains less accessible due to higher mass transfer resistance.

Reverchon [6] formulated a fluid-solid extraction model where the solute is treated as a single component, governed by internal mass transfer resistance and omitting the effects of external mass transfer, axial dispersion, and variations in fluid density and flow rate throughout the bed.

This work builds upon the linear kinetic model suggested by Reverchon [6], deriving fundamental governing equations to develop a comprehensive model for the chamomile oil extraction process. This model aims for control-oriented simplicity, assuming a semi-continuous operation within a cylindrical vessel. The process involves supercritical solvent being pumped through a fixed bed of finely chopped biomass to extract the solute, followed by separation of the solvent and solute in a flush drum to collect the extract. Parameters such as the pressure (P), feed flow rate (F_{in}) and inlet temperature (T_{in}) are adjustable

*Corresponding author
oliwer.sliczniuk@aalto.fi (O. Sliczniuk)
ORCID(s): 0000-0003-2593-5956 (O. Sliczniuk); 0000-0002-0183-5558 (P. Oinas)

and measurable, while the outlet temperature (T_{out}) and the amount of product at the outlet can only be monitored. Figure 1 presents a simplified process flow diagram.

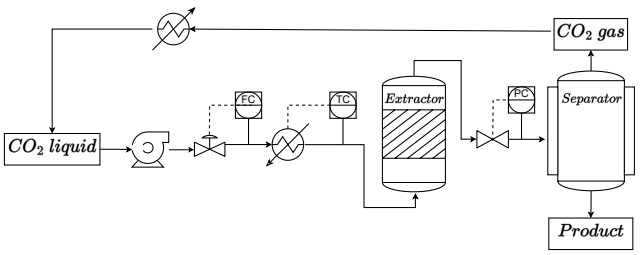

Figure 1: Process flow diagram

This study focuses on finding a process model for the extraction of natural substances from solid materials using supercritical fluids, with a particular emphasis on supercritical CO_2. The approach involves estimating the solvent properties through thermodynamic relationships and determining the extraction kinetic parameters via a series of experiments conducted under a variety of conditions. The maximum likelihood estimation method is employed solve the parameter estimation problem. Later, the correlations between parameters and operating conditions are found.

2. Materials and methods

2.1. Governing equations

The governing equations based on the work of Anderson [7] for quasi-one-dimensional compressible flow in Cartesian coordinates are presented in Appendix A.1. Quasi-one-dimensional flow refers to a fluid flow scenario assuming that flow properties are uniformly distributed across any given cross-section. This simplification is typically applied in situations where the flow channel's cross-sectional area changes, such as through irregular shapes or partial fillings of an extractor. According to this assumption, velocity and other flow properties change solely in the flow direction.

The set of quasi-one-dimensional compressible Navier-Stokes equations in Cartesian coordinates is described by Equations 1 - 3. The formulation of these equations is elaborated upon in Appendix A.1, providing a mathematical foundation for analyzing flow dynamics under the assumed conditions.

$$\frac{\partial\left(\rho_f A_f\right)}{\partial t}+\frac{\partial\left(\rho_f A_f v\right)}{\partial z}=0 \tag{1}$$

$$\frac{\partial\left(\rho_f v A_f\right)}{\partial t}+\frac{\partial\left(\rho_f A_f v^2\right)}{\partial z}=-A_f\frac{\partial P}{\partial z} \tag{2}$$

$$\frac{\partial\left(\rho_f e A_f\right)}{\partial t}+\frac{\partial\left(\rho_f A_f v e\right)}{\partial z}=-P\frac{\left(A_f v\right)}{\partial z}+\frac{\partial}{\partial z}\left(k\frac{\partial T}{\partial z}\right) \tag{3}$$

where ρ_f is the density of the fluid, A_f is the function which describe change of the cross-section, v is the velocity, P is the total pressure, e is the internal energy of the fluid, t is time and z is the spacial direction.

Based on governing equations, the small discontinuity (defined as δ) in flow properties, shown in Figure 2, can be analysed. The analysis follows the work of Schreier [8].

	ρ_f	$\rho_f+\delta\rho_f$	
$v\rightarrow$	P	$P+\delta P$	$v+\delta v\rightarrow$
	T	$T+\delta T$	

Figure 2: Small discontinuity in one-dimensional flow

The discontinuity is presumed to be at rest relative, and the balance equations become

$$\rho_f\delta v+v\delta\rho_f+\delta\rho_f\delta v=0$$
$$\delta P=\delta v\delta\rho_f$$

These relations are equally valid if both regions are separated by a region of finite width rather than a discontinuity.

$$\lim_{\rho_f v\rightarrow 0}\rho_f\delta v+v\delta\rho_f+\delta\rho_f\delta v=0/\delta\rho_f\rightarrow\frac{dv}{d\rho_f}=-\frac{v}{\rho_f}$$

By combining the momentum equation with the above equation, we get

$$\frac{dv}{d\rho_f}=-\frac{dv}{dP}\frac{dP}{d\rho_f}=-\frac{1}{\rho v}\frac{dP}{d\rho_f}=-\frac{v}{\rho_f} \tag{4}$$

Suppose the flow is presumed to be isentropic, $dP/d\rho_f = c^2$, so $v^2 = c^2$, where c is the speed of sound. This can be interpreted as a small pressure wave propagating with the speed of sound relative to the flow. If the flow velocity is relatively low, all pressure changes are hydrodynamic (due to velocity motion) rather than thermodynamic, which leads to $\partial\rho_f/\partial P\approx 0$. The small changes in pressure due to flow velocity changes do not change the density.

The low Mach number condition leads to the incompressible condition: $\nabla\cdot u=0$, which is valid for constant density (strict incompressible) or varying density flow. The restraint allows for the removal of acoustic waves, but also allows for large perturbations in density and/or temperature. The assumption is that the flow remains within a Mach number limit (usually less than 0.3) for any solution using such a constraint to be valid. In the 1-D case, the incompressibility condition becomes $\frac{du}{dz}=0$, so the fluid velocity is constant.

2.2. Extraction model

2.2.1. Continuity equation

The previously derived quasi-one-dimensional continuity equation (Equation 1) is refined by incorporating a function $A_f = A\phi$. This modification accounts for the variability in the cross-sectional area available for fluid flow. Equation 5 presents this adaptation in the differential form of the continuity equation, capturing the dynamics of the flow as it responds to changes in the cross-section.

$$\frac{\partial(\rho_f\phi)}{\partial t}+\frac{\partial(\rho_f v A\phi)}{\partial z}=0 \tag{5}$$

where A is the total cross-section of the extractor and ϕ describe porosity along the extractor.

Assuming that the mass flow rate is constant in time, the temporal derivative becomes the mass flux F, and the spatial derivative can be integrated along z as

$$\int \frac{\partial(\rho_f v A\phi)}{\partial z} dz = F \rightarrow F = \rho_f v A\phi \tag{6}$$

To simplify the system's dynamics, it is assumed that F is a control variable and affects the whole system instantaneously, which allows finding the velocity profile that satisfies mass continuity based on F, ϕ, and ρ_f.

$$v = \frac{F}{\rho_f A\phi} \tag{7}$$

Similarly, the superficial velocity might be introduced.

$$u = v\phi = \frac{F}{\rho_f A} \tag{8}$$

The fluid density ρ_f can be obtained from an equation of state (Appendix A.2) if temperature and thermodynamic pressure are known along z. The variation in fluid density may occurs due to pressure or a inlet temperature changes.

2.2.2. Mass balance for the fluid phase

The comprehensive derivation of the mass balance equation for the fluid phase is detailed in Appendix A.1. This equation accounts for the movement of the pseudo-homogeneous fluid phase (Equation 9), which is constrained to the axial direction due to the quasi-one-dimensional approach that considers changes in the void fraction. It is also assumed that the thermodynamic pressure remains constant throughout the device, as illustrated by Equation 4. The analysis further simplifies the flow dynamics by disregarding the boundary layer near the extractor's inner wall, leading to a uniform velocity profile across any cross-section perpendicular to the axial direction. Given that the solute concentration in the solvent is negligible, the fluid phase is described as pseudo-homogeneous, with properties identical to the solvent itself. Thus, the mass balance equation encompasses convection, diffusion, and kinetic terms to represent the fluid phase behaviour accurately.

$$\frac{\partial c_f}{\partial t} + \frac{1}{\phi}\frac{\partial\left(c_f u\right)}{\partial z} = \frac{1-\phi}{\phi} r_e + \frac{1}{\phi}\frac{\partial}{\partial z}\left(D_e^M \frac{\partial c_f}{\partial z}\right) \tag{9}$$

c_f represents the concentration of solute in the fluid phase, r_e is a mass transfer kinetic term, and D_e^M is the axial diffusion coefficient.

2.2.3. Mass balance for the solid phase

The solid phase is considered to be stationary, without convection and diffusion terms in the mass balance equation (Equation 10). Therefore, the only significant term in this equation is the kinetic term (as defined in Equation 11), which connects the solid and fluid phases. The extract is represented by a single pseudo-component for simplicity.

$$\frac{\partial c_s}{\partial t} = \underbrace{r_e}_{\text{Kinetics}} \tag{10}$$

2.2.4. Kinetic term

The kinetic term in this study is based on the two-film theory proposed by Reverchon [6], and the mass transfer kinetic is given by Equation 11. This equation takes into account the overall diffusion coefficient and the concentration gradient, which acts as the driving force for the process.

As the solvent flows through the bed, CO_2 molecules diffuse into the pores and adsorb on the particle surface to form an external fluid film around the solid particles due to the solvent-solid matrix interactions. The dissolved solute diffuses from the particle's core through the solid-fluid interface, the pore, and the film into the bulk. Figure 3 illustrates the mass transfer mechanism, where the mean solute concentration in the solid phase is denoted as c_s and the equilibrium concentrations at the solid-fluid interface are denoted as c_s^* and c_p^*, respectively, for solid and fluid phases. The concentration of the solutes in the fluid phase in the center of the pore is denoted as c_p. As the solute diffuses through the pore, its concentration changes and reaches c_{pf} at the opening of the pore. The solute then diffuses through the film around the particle and reaches bulk concentration c_f. The two-film theory describes the solid-fluid interface inside the pore. The overall mass transfer coefficient can be determined if the relationship between the solute concentration in one phase and its equilibrium concentration is known.

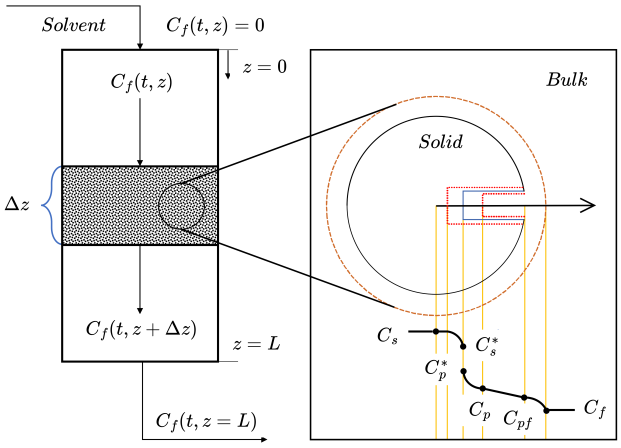

Figure 3: The extraction mechanism

Bulley et al. [9] suggests a process where the driving force for extraction is given by the difference between the concentration of the solute in bulk, c_f, and in the center of the pore, c_p^*. The concentration c_p^* is in equilibrium with c_s according to an equilibrium relationship. The rate of extraction is thus $r_e\left(c_f - c_p^*(c_s)\right)$.

On the other hand, Reverchon [6] proposes a driving force given by the difference between c_s and c_p^*. c_p^* is determined by an equilibrium relationship with c_f and the extraction rate is $r_e\left(c_s - c_p^*(c_f)\right)$ or more precisely

$$r_e = \frac{D_i}{\mu l^2}\left(c_s - c_p^*\right) \tag{11}$$

where μ is sphericity, l a characteristic dimension of particles and can be defined as $l = r/3$, r is the mean particle radius, ρ_s is the solid density, D_i corresponds to the overall

diffusion coefficient and c_P^* is a concentration at the solid-fluid interface (which according to the internal resistance model is supposed to be at equilibrium with the fluid phase).

According to Bulley et al. [9], a linear equilibrium relationship (Equation 12) can be used to find an equilibrium concentration of the solute in the fluid phase c_f^* is based on the concentration of the solute in the solid phase c_s.

$$c_f^* = k_p c_s \tag{12}$$

The volumetric partition coefficient k_p acts as an equilibrium constant between the solute concentration in one phase and the corresponding equilibrium concentration at the solid-fluid interphase. According to Spiro [10], k_p can be expressed through the mass partition coefficient k_m.

$$k_m = \frac{k_p \rho_s}{\rho_f} \tag{13}$$

According to Reverchon [6], the kinetic term becomes

$$r_e = -\frac{D_i}{\mu l^2}\left(c_s - \frac{\rho_s c_f}{k_m \rho_f}\right) \tag{14}$$

2.2.5. Uneven solute's distribution in the solid phase

Following the idea of the Broken-and-Intact Cell (BIC) model (Sovova [11]), the internal diffusion coefficient D_i is consider to be a product of the reference value of D_i^R and the exponential decay function γ, as given by Equation 15.

$$D_i = D_i^R \gamma(c_s) = D_i^R \exp\left(\Upsilon\left(1 - \frac{c_s}{c_{s0}}\right)\right) \tag{15}$$

where the Υ describe the curvature of the decay function. Equation 16 describes the final form of the kinetic term

$$r_e = -\frac{D_i^R \gamma}{\mu l^2}\left(c_s - \frac{\rho_s c_f}{k_m \rho_f}\right) \tag{16}$$

Such a formulation limits the availability of the solute in the solid phase. Similarly to the BIC model, if solute is assumed to be contained in the cells, a part of which is open because the cell walls were broken by grinding, and the rest remains intact. The diffusion of the solute from a particle's core takes more time compared to the diffusion of the solute located close to the outer surface. Considering that the internal diffusion coefficient decay as the concentration of the solute in the solid decrease. As the value of the c_s decrease over time, the exponential term approach unity and $\lim_{c_s \to 0} D_i = D_i^R$. D_i^R can be interpreted as the internal diffusion coefficient at vanishing gradient.

Alternatively, the decay function γ can be consider with respect to the Shrinking Core model presented by Goto et al. [12], where the particle radius change as the amount of solute in the solid phase decrease. As the particle size decrease due to dissolution, the diffusion path increase which makes the diffusion slower and reduce the value of a diffusion coefficient. The same analogy can be apply to the Equation 15 to explain the change of the diffusion coefficient.

2.2.6. Extraction yield

The efficiency of the process (the yield) is calculated according to Equation 17 as presented by Sovova et al. [13]. The measurement equation evaluates the solute's mass at the extraction unit's outlet and sums it up. The integral form of the measurement equation (17) can be transformed into the differential form (18) and augmented with the process model.

$$y = \int_{t_0}^{t_f} \frac{F}{\rho_f} c_f \Big|_{z=L} dt \tag{17}$$

$$\frac{dy}{dt} = \frac{F}{\rho_f} c_f \Big|_{z=L} \tag{18}$$

2.2.7. Initial and boundary conditions

It is assumed that the solvent is free of solute at the entrance of the extractor and that all the solid particles have the same initial solute content c_{s0}. As the residence time is much shorter than the sampling time, the initial state estimate for the concentration of the solute in the fluid phase would be not reliable. Considering that it is assumed that the $c_{f0} = 0$. Moreover, it is considered that the extractor is isothermal. Therefore, the initial and boundary conditions employed in the simulation are:

$$c_f(t=0,z) = 0 \qquad c_s(t=0,z) = c_{s0} \qquad c_f(t,z=0) = 0$$
$$\frac{\partial c_f(t,z=L)}{\partial x} = 0 \qquad c_s(t,z=\{0,L\}) = 0 \qquad y(0) = 0$$

2.2.8. Discretization methods

The method of lines is used to transform the process model equations into a set of ODEs denoted as $G(x;\Theta)$. The backward finite difference is used to approximate the first-order derivative, while the central difference scheme is used to approximate the second-order derivative z-direction. The length of the fixed bed is divided into N_z equally distributed points in z-direction. The state-space model after the discretization is represented by x.

$$\dot{x} = \frac{dx}{dt} = \begin{bmatrix} \frac{dc_{f,1}}{dt} \\ \vdots \\ \frac{dc_{f,N_z}}{dt} \\ \hline \frac{dc_{s,1}}{dt} \\ \vdots \\ \frac{dc_{s,N_z}}{dt} \\ \hline \frac{dy(t)}{dt} \end{bmatrix} = \underbrace{\begin{bmatrix} G_1\left(c_f, c_s; \Theta\right) \\ \vdots \\ G_{N_z}\left(c_f, c_s; \Theta\right) \\ \hline G_{N_z+1}\left(c_f, c_s; \Theta\right) \\ \vdots \\ G_{2N_z}\left(c_f, c_s; \Theta\right) \\ \hline G_{2N_z+2}\left(c_f, c_s; \Theta\right) \end{bmatrix}}_{G(x;\Theta)}$$

where $x \in \mathbb{R}^{N_x = 2N_z+1}$ and $\Theta \in \mathbb{R}^{N_\Theta = N_\theta + N_u}$, N_θ is the number of parameters, N_u is the number of control variables.

As presented in Appendix A.1, all the governing can be written in the integral form using the Divergence Theorem. The integral equation states that the change rate of the integral of any quantity over an arbitrary control volume

is given by the flux through the boundary of the control volume, with being the outer surface normal through the boundary. That quantity is conserved and neither produced nor consumed inside the control volume. For a derivative to be conservative, it must form a telescoping series. In other words, after the addition of all terms coming from the discretization over a grid, only the boundary terms should remain, and the artificial interior points should cancel out. Discretization is applied to the conservative form of the process model to ensure mass conservation.

2.3. Parameter estimation

Only some of the parameters in a process model can be estimated from the theoretical considerations. The goal of parameter estimation is to obtain the "best" estimate of unknown parameters θ (which is a subset of the parameter space Θ containing all parameters of a model) based on the continuous observations $Y(t)$ or the discrete observations $Y(t_i)$. Conceptually, the unobservable error $\epsilon(t)$ is added to the deterministic model output, $y(t)$ (Equation 17), to give the observable dependent variable $Y(t)$ (for example results of an experiment). For discrete observations, this can be expressed as:

$$Y(t_i) = y(\theta, t_i) + \epsilon(t_i)$$

For continuous variables, the equation is:

$$Y(t) = y(\theta, t) + \epsilon(t)$$

However, obtaining analytical solutions for a deterministic process model can be challenging, so experiments are often conducted where the vector of derivatives $dY(t_i)/dt$ is measured instead of $Y(t_i)$ itself. In such cases, it is assumed that the unobservable error is added to the deterministic derivative $dy(\theta, t_i)/dt$ as shown below

$$\frac{dY(t_i)}{dt} = \frac{dy(\theta, t_i)}{dt} + \epsilon(t_i) \tag{19}$$

In the case where the error in the first observation is denoted as ϵ_1, the error in the second observation ϵ_2' incorporates ϵ_1 as well as an independent random component, given by $\epsilon_2' = \epsilon_1 + \epsilon_2$. Similarly, the error in the third observation is $\epsilon_3' = \epsilon_1 + \epsilon_2 + \epsilon_3$, etc. Mandel [14] made a distinction between the typically assumed independent measurement error in the dependent variable and a "cumulative" or interval error, in which each new observation encompasses the error of the previous ones. Cumulative errors arise from fluctuations in the process due to small variations in operating conditions and are not independent; only the differences in measurement from one period to the next are independent.

Maximum likelihood estimation (MLE) is a statistical method used to estimate the parameters of a probability distribution based on observed data. The MLE works by finding the values of the parameters that maximize the likelihood function, which is the probability of observing the given data for a given set of parameter values. The MLE has desirable properties such as asymptotic efficiency and normality. Although the MLE has often been associated with the normal distribution for mathematical convenience, it can be applied to a wide range of probability distributions. The derivation of the likelihood function under the assumption of the Gaussian distribution is presented in Appendix A.4. The objective function is presented by Equation 20:

$$\ln L = -\frac{n}{2}\ln\left(2\pi\sigma^2\right) - \frac{\sum_{i=1}^{n}\left[\frac{dY(t_i)}{dt} - \frac{dy(\theta, t_i)}{dt}\right]^2}{2\sigma^2} \tag{20}$$

The parameter estimation problem can be formulated as follow:

$$\begin{aligned} \hat{\theta}_{MLE} &= \arg\max_{\sigma,\theta\in\Theta} \ln L = \arg\max_{\sigma,\theta\in\Theta} p(\theta|y) \\ \text{subject to} \quad \dot{x} &= G(x(t);\theta) \\ \dot{\theta} &= 0 \\ y &= y(t) \\ \theta^{lb} &\le \theta \le \theta^{ub} \end{aligned} \tag{21}$$

where $\hat{\theta}$ is as maximum likelihood estimator, θ^{lb} define the minimal value of θ, θ^{ub} is the maximum value of θ and σ represents the standard deviation of the residuals (errors) between the observed data points and the model outputs.

The initial guess for each decision variable, as well as the lower and upper bounds are given in Table 1.

Parameter	k_m[-]	$D_i^R \times 10^{-13}[m^2/s]$	$D_e^M \times 10^{-12}[m^2/s]$	Υ [-]
Lower bound	0	0	0	0
Upper bound	$+\infty$	$+\infty$	$+\infty$	$+\infty$
Initial guesses	0.1-10	$0.1 - 10$	0.1-10	0.1-10

Table 1: Constraints and initial guess

Solution of Equations 21 yield the desired estimates $\hat{\theta}$. For some models, these equations can be explicitly solved for $\hat{\theta}$ but in general, no closed-form solution to the maximization problem is known or available, and a maximum likelihood estimator can only be found via numerical optimization.

2.4. Experimental work

The experiments were conducted using an a semi-batch extractor with diameter of 3.96 [cm] and length of 16.55 [cm]. Twelve experiments were performed under different operating conditions: $30 - 40°C$, $100 - 200$ [bar], and $0.05 - 0.24$ [kg/h]. The amount of solid material used for extraction was 75 [g], which was sufficient to fill the whole vessel. The bulk density of the bed was computed based on the feed's mass and the extractor's volume. The total porosity of the bed, including the particles, was determined using the following calculation: $\epsilon = 1 - \frac{d_a}{d_r} = 1 - \frac{370}{1364} = 0.73$.

3. Results

To solve the parameter estimation problem, the single shooting method was used to transform the boundary-value problem into the initial value problem and to formulate the non-linear programming problem. This non-linear optimization task was tackled using the CasADi framework (Andersson et al. [17]). Each time series was fitted separately to the model with the linear extraction kinetics (Equation 14). The initial value problem was solved multiple times with varying initial guesses to identify the global minimum.

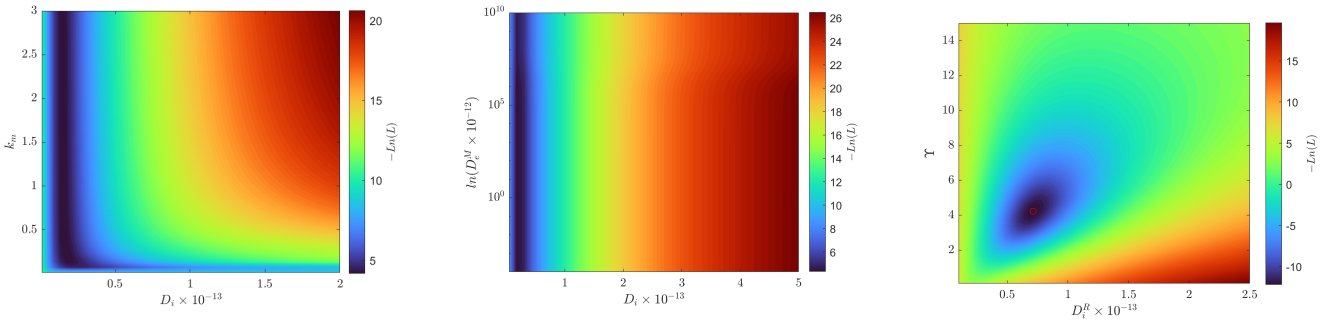

(a) Parameter space: the linear kinetic model

(b) Parameter space: the reduced linear kinetic model with axial diffusion

(c) Parameter space: the modified model

Figure 4: Parameter estimation results for experiment 1

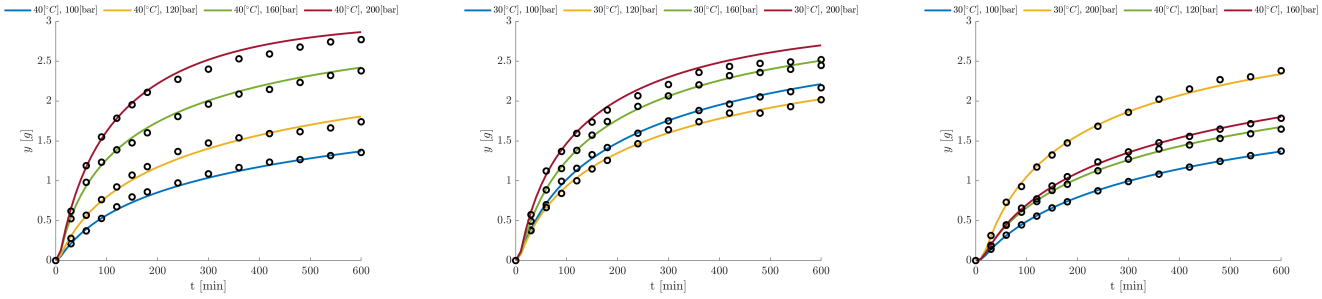

(a) Parameter estimation results at 6.67×10^{-5} [kg/s] and temperature of 40 [$°C$]

(b) Parameter estimation results at 6.67×10^{-5} [kg/s] and temperature of 30 [$°C$]

(c) Results of parameter estimation for experiments at 3.33×10^{-5} [kg/s]

Figure 5: Parameter estimation results

Within the model context characterized by linear kinetics, two parameters remain to be determined: the partition coefficient k_m and the internal diffusion coefficient D_i.

Figure 4a shows the parameter space and corresponding values of the cost function for experiment 1 (40$°C$, 100 bar and 6.67×10^{-5} kg/s). As the cost function is to be minimized, the lowest value of $-\ln(L)$ indicate the best fit. A black vertical stripe at $D_i \approx 0.2$ can be observed. That stripe indicates the existence of the optimal value of the D_i. In the direction of k_m, the cost function is almost flat, which suggests that any value of k_m above 0.1 fits the data equally well. If k_m can be an arbitrary point, then it can grow to infinity, which suggests that the solvent is far from the saturation, and the model can be simplified. The model reduction can be introduced by considering the limit of k_m in the extraction kinetic term:

$$\lim_{k_m \to \infty} \left(c_s(t,z) - \frac{\rho_s}{k_m(T(t,z))\rho(T(t,z),P(t))} c_f \right) =$$

$$= \left(c_s(t,z) - \frac{\rho_s}{\infty \cdot \rho(T(t,z),P(t))} c_f(t,z) \right) = \left(c_s(t,z) - 0 \right)$$

The extraction model can be adapted to incorporate adjustments for the reduced kinetic term and axial diffusion. In this revised setup, two parameters remain undetermined: the internal diffusion coefficient D_i and the axial diffusion coefficient D_e^M. Figure 4b illustrates the parameter space and associated cost function values.

Similarly to the previous case, the optimal value of D_i exists, but a unique value for the D_e^M cannot be determined. Figure 4b illustrates the minimal impact of the axial diffusion coefficient, where a broad range of D_e^M yields identical cost function values. By selecting a low value D_e^M, the axial diffusion terms can be reduced or eliminated from the model without compromising its generality. This observation aligns with the findings of Rahimi et al. [16], who analysed the same dataset and reported Peclet numbers ranging between 290 and 400. Such high values of the Peclet number suggest that the advection term dominates the mass transfer, and the axial diffusion is negligible.

In both scenarios previously discussed, the fitting outcomes were not deemed satisfactory. Building upon the concepts underlying the Broken-and-Intact and Shrinking Core models (detailed in Chapter 2.2.5), the gamma function is introduced to capture the decreasing extraction kinetics. The correction factor is combined with the simplified linear model, resulting in a two-parameter model (D_i^R and Υ) as given by Equation 16. Figure 4c shows the parameter space and the corresponding cost function values.

The parameter space for the revised model exhibits a distinct minimum value corresponding to the solution of the parameter estimation problem for experiment 1. The red circle highlights the minimum value of the cost function found by the optimizer. The remaining experiments are fitted to the modified extraction model, and results are presented

in Figure 5. The obtained results show good agreement with experimental data.

The parameter estimation results are combined to analyse the relationship between the obtained parameters and the operating conditions. Unlike traditional methods that employ a combination of Reynolds, Schmidt, and Sherwood numbers to find correlations—omitted here due to the insignificance of axial diffusion—the approach in this study leverages the Reynolds number $\left(Re = \frac{(2r)\cdot\rho_f\cdot u}{\mu}\right)$ as the sole independent variable. Using the Reynolds number has the advantage of considering the influence of all the control variables (temperature, pressure and flow rate), which means it can be uniquely defined by selecting operating conditions.

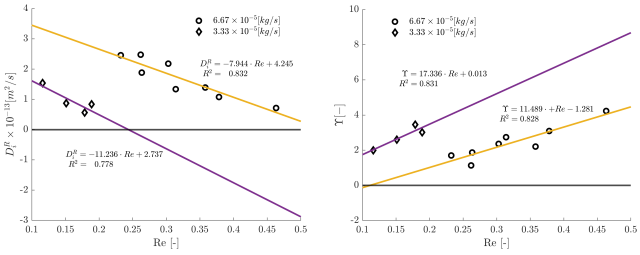

(a) Linear regression $D_i^R = f(Re)$

(b) Linear regression $\Upsilon = f(Re)$

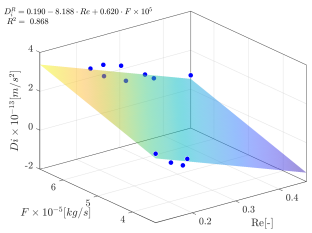

(c) Multiple linear regression $D_i^R = f(Re, F)$

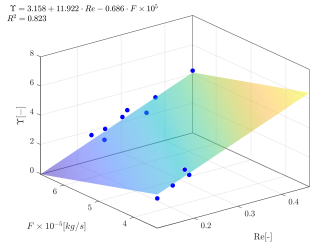

(d) Multiple linear regression $\Upsilon = f(Re, F)$

Figure 6: Parameter estimation results

In Figures 6a and 6b, two distinct data clusters emerge, each corresponding to a different mass flow rate. Despite the linear trends observed in both sets of correlations, the correlations for D_i^R exhibit a decline with increasing Re, whereas those for Υ show an upward trend with Re. The decrease in D_i^R across each data line can be attributed to higher fluid density and increased mass transfer resistance.

A more general relationship can be obtained by applying multiple linear regression instead of linear regression. The clusters in Figure 6a and 6b are close to parallel, suggesting that a plane would combine all the data points. The Reynolds number and flow rate act as independent variables for D_i^R and Υ as presented in Figures 6c and 6d. The presented correlations are valid in the whole range of investigated operating conditions.

The correlations are later used against the original dataset to show that the correlations can reproduce the results with satisfactory accuracy. Figure 7 shows the results of the simulations with incorporated correlations. A good agreement between simulation results and the dataset can be observed. If Figures 5 and 7 are compared, a decrease in the accuracy of simulations can be observed. Such a behaviour is expected due the bias–variance trade-off, which describes the relationship between a model's complexity and the accuracy of its predictions.

4. Conclusions

The article presents a comprehensive study on supercritical fluid extraction of essential oil from chamomile flowers, focusing on developing and applying a distributed-parameter model to describe the fluid-solid extraction process. By employing the concept of quasi-one-dimensional flow, the study simplifies the spatial dimensions of the extraction process, ensuring uniform flow across any cross-section while allowing for variations in the area available for the fluid phase. The physical properties of the solvent are estimated using the Peng-Robinson equation of state, and key model parameters are determined through maximum likelihood estimation based on experimental data, considering normally distributed errors.

Laboratory experiments were conducted by Povh et al. [15] under various conditions to validate the model. The model parameters, such as partition factor, internal diffusion coefficient, axial diffusion coefficient, and decaying factor, were determined through maximum likelihood estimation based on experimental data. The parameter space exploration revealed that while some parameters could be determined with a high degree of confidence, others, like the axial diffusion coefficient, had a low impact on the model's output. The identification of the low-impact parameters leads to model reduction

This work introduced a set of correlations to find a general relationship between parameters and the independent variables, which can be determined by operating conditions. The obtained correlations were introduced into the model and tested against the dataset. The results show good agreement between the simulation results and all the data points.

The presented model can be further used with the presented correlations to introduce an extraction model with dynamically changing operating conditions for multiple purposes, such as yield maximisation, techno-economic analysis, or optimal experiments design.

References

[1] Ompal Singh, Zakia Khanam, Neelam Misra, and ManojKumar Srivastava. Chamomile (matricaria chamomilla l.): An overview. Pharmacognosy Reviews, 5(9):82, 2011. ISSN 0973-7847. doi: 10.4103/0973-7847.79103.

[2] Janmejai Srivastava. Extraction, characterization, stability and biological activity of flavonoids isolated from chamomile flowers. Molecular and Cellular Pharmacology, 1(3):138–147, August 2009. ISSN 1938-1247. doi: 10.4255/mcpharmacol.09.18.

[3] Anne Orav, Ain Raal, and Elmar Arak. Content and composition of the essential oil ofchamomilla recutita(l.) rauschert from some european countries. Natural Product Research, 24(1):48–55, January 2010. ISSN 1478-6427. doi: 10.1080/14786410802560690.

[4] Ernesto Reverchon, Giorgio Donsi, and Libero Sesti Osseo. Modeling of supercritical fluid extraction from herbaceous matrices. Industrial

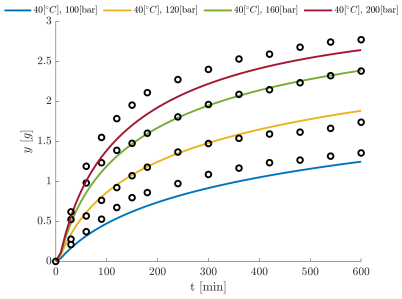

(a) Parameter estimation results at 6.67×10^{-5} [kg/s] and temperature of 40 [$°C$]

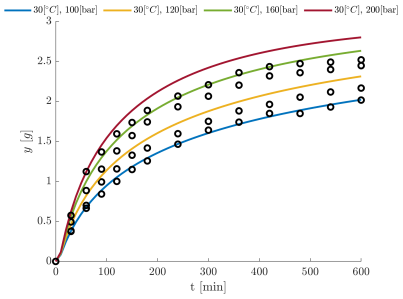

(b) Parameter estimation results at 6.67×10^{-5} [kg/s] and temperature of 30 [$°C$]

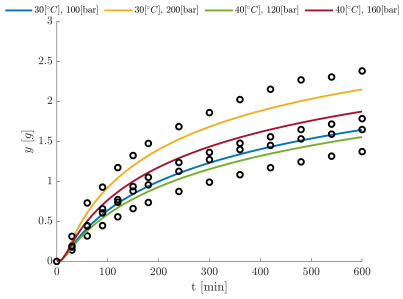

(c) Results of parameter estimation for experiments at 3.33×10^{-5} [kg/s]

Figure 7: Parameter estimation results

& Engineering Chemistry Research, 32(11):2721–2726, nov 1993. doi: 10.1021/ie00023a039.

[5] Helena Sovova. Rate of the vegetable oil extraction with supercritical co2. modelling of extraction curves. Chemical Engineering Science, 49(3):409–414, 1994. doi: 10.1016/0009-2509(94)87012-8.

[6] Ernesto Reverchon. Mathematical modeling of supercritical extraction of sage oil. AIChE Journal, 42(6):1765–1771, jun 1996. doi: 10.1002/aic.690420627.

[7] John D. Anderson. Computational fluid dynamics the basic with applications. McGraw-Hill, 1995. ISBN 9780071132107.

[8] Stefan Schreier. Compressible flow. Wiley, 1982. ISBN 047105691X.

[9] N. R. Bulley, M. Fattori, A. Meisen, and L. Moyls. Supercritical fluid extraction of vegetable oil seeds. Journal of the American Oil Chemists' Society, 61(8):1362–1365, aug 1984. doi: 10.1007/bf02542243.

[10] M. Spiro. Extraction of ginger rhizome: partition constants and other equilibrium properties in organic solvents and in supercritical carbon dioxide. International Journal of Food Science & Technology, 25(5):566–575, jun 2007. doi: 10.1111/j.1365-2621.1990.tb01116.x.

[11] Helena Sovova. Broken-and-intact cell model for supercritical fluid extraction: Its origin and limits. The Journal of Supercritical Fluids, 129:3–8, nov 2017. doi: 10.1016/j.supflu.2017.02.014.

[12] Motonobu Goto, Bhupesh C. Roy, and Tsutomu Hirose. Shrinking-core leaching model for supercritical-fluid extraction. The Journal of Supercritical Fluids, 9(2):128–133, jun 1996. doi: 10.1016/s0896-8446(96)90009-1.

[13] Helena Sovova, Radko Komers, J. Kucuera, and Jaromir Jezu. Supercritical carbon dioxide extraction of caraway essential oil. Chemical Engineering Science, 49(15):2499–2505, aug 1994. doi: 10.1016/0009-2509(94)e0058-x.

[14] John Mandel. Fitting a straight line to certain types of cumulative data. Journal of the American Statistical Association, 52(280):552–566, dec 1957. doi: 10.1080/01621459.1957.10501413.

[15] Nanci P. Povh, Marcia O.M. Marques, and M.Angela A. Meireles. Supercritical co2 extraction of essential oil and oleoresin from chamomile (chamomilla recutita [l.] rauschert). The Journal of Supercritical Fluids, 21(3):245–256, November 2001. ISSN 0896-8446. doi: 10.1016/s0896-8446(01)00096-1.

[16] E. Rahimi, J.M. Prado, G. Zahedi, and M.A.A. Meireles. Chamomile extraction with supercritical carbon dioxide: Mathematical modeling and optimization. The Journal of Supercritical Fluids, 56(1):80–88, February 2011. ISSN 0896-8446. doi: 10.1016/j.supflu.2010.11.008.

[17] Joel A. E. Andersson, Joris Gillis, Greg Horn, James B. Rawlings, and Moritz Diehl. CasADi: a software framework for nonlinear optimization and optimal control. Mathematical Programming Computation, 11(1):1–36, jul 2018. doi: 10.1007/s12532-018-0139-4.

[18] Ding-Yu Peng and Donald B. Robinson. A new two-constant equation of state. Industrial & Engineering Chemistry Fundamentals, 15(1):59–64, feb 1976. doi: 10.1021/i160057a011.

[19] Jürgen Gmehling, Michael Kleiber, Bärbel Kolbe, and Jürgen Rarey. Chemical Thermodynamics for Process Simulation. Wiley, mar 2019. doi: 10.1002/9783527809479.

A. Appendix

A.1. Governing equations

A.1.1. Mass continuity

Following the work of Anderson [7], the governing equations for compressible fluid with non-uniform cross-section can be obtained. Let's assume that any properties of the flow are uniform across any given cross-section of an extractor. The variation of the cross-section might result from the partial filling of an extractor or its irregular shape. In reality, such a flow is two-dimensional because the area changes as a function of z, and there is a flow-field variation in both directions. The assumption of quasi-one-dimensional flow dictates that the flow properties are a function of z only. The integral form of the continuity equation is:

$$\frac{\partial}{\partial t}\iiint_{\mathcal{V}_f} \rho_f d\mathcal{V}_f + \iint_S \rho_f \mathbf{V}\cdot\mathbf{dS} = 0 \tag{22}$$

We apply this equation to the shaded control volume shown in Figure 8.

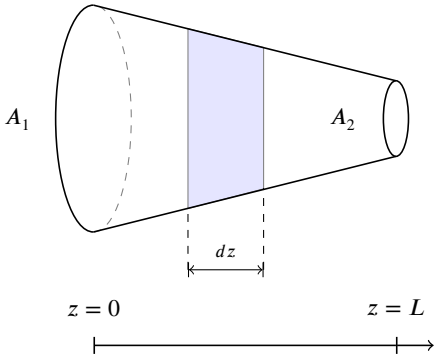

Figure 8: Control volume for deriving the partial differential equation for unsteady, quasi-one-dimensional flow

On the left side of the control volume, consistent with the quasi-one-dimensional assumptions, the density, velocity, pressure, and internal energy denoted by ρ_f, v, P, and e, respectively, are uniform over the area A. Similarly, on the right side of the control volume, the density, velocity, pressure, and internal energy $\rho_f + d\rho_f$, $v + dv$, $P + dP$, and $e + de$, respectively, are uniform over the area available for fluid phase $A_f + dA_f$. Applied to the control volume in Figure 8, the volume integral in Equation 22 becomes, in the limit as dz becomes very small,

$$\frac{\partial}{\partial t}\iiint_{\mathcal{V}_f} \rho_f d\mathcal{V}_f = \frac{\partial}{\partial t}\left(\rho_f A_f dz\right) \tag{23}$$

where $A\,dz$ is the volume of the control volume in the limit of dz becoming vanishingly small. The surface integral in Equation 22 becomes

$$\iint_S \rho_f \mathbf{V}\cdot\mathbf{dS} = -\rho_f v A_f + (\rho_f + d\rho_f)(v + dv)(A_f + dA_f) \tag{24}$$

The minus sign on the leading term on the right-hand side is due to the vectors $\mathbf{V}$ and $\mathbf{dS}$ pointing in opposite directions over the left of the control volume, and hence the dot product is negative. Expanding the triple product term

$$\begin{aligned}\iint_S \rho_f \mathbf{V}\cdot\mathbf{dS} &= -\rho_f v A_f + \rho_f v A_f + \rho_f v dA_f + \rho_f A_f dv \\ &+ \rho_f dv dA_f + v A_f d\rho_f + v d\rho_f dA + A_f d\rho_f dv + d\rho_f dv dA_f\end{aligned} \tag{25}$$

In the limit as dz becomes very small, the terms involving products of the differential in Equation 25, such as $\rho_f dv dA_f$, $d\rho_f dv dA_f$, go to zero much faster than those terms involving only one differential. Hence, all terms involving products of differentials can be dropped, yielding in the limit as dz becomes very small

$$\iint_S \rho_f \mathbf{V}\cdot\mathbf{dS} = \rho_f v dA_f + \rho_f A_f dv + v A_f d\rho_f \tag{26}$$

Substituting Eqs. 23 and 26 into 22, we have

$$\frac{\partial\left(\rho_f A_f\right)}{\partial t} + \frac{\partial\left(\rho_f A_f v\right)}{\partial z} = 0 \tag{27}$$

The above partial differential equation form of the continuity equation is suitable for unsteady, quasi-one-dimensional flow. The $A_f(z)$ is an arbitrary function that describes a change in the extractor's cross-section and can be defined as $A_f(z) = \mathbf{A}\phi(z)$, where ϕ is the bed porosity and $\mathbf{A}$ is the cross-section of an empty extractor.

$$\frac{\partial\left(\rho_f \mathbf{A}\phi(z)\right)}{\partial t} + \frac{\partial\left(\rho_f \mathbf{A}\phi(z)v\right)}{\partial z} = 0 \tag{28}$$

The equation can be simplified by canceling out $\mathbf{A}$

$$\frac{\partial\left(\rho_f \phi(z)\right)}{\partial t} + \frac{\partial\left(\rho_f \phi(z)v\right)}{\partial z} = 0 \tag{29}$$

If so-called superficial velocity is defined as $u = \phi v$, the mass continuity becomes

$$\frac{\partial\left(\rho_f \phi(z)\right)}{\partial t} + \frac{\partial\left(\rho_f u\right)}{\partial z} = 0 \tag{30}$$

A.1.2. Transport of a species

The transport of a solute, can be described by an analogous equation to the Equation 22 with additional terms on the right-hand side. The first term on the right-hand side describes diffusional movement of species and is based on the Fick's law $\left(J_{diff} = D_e^M \frac{\partial c_f}{\partial z}\right)$. The other term corresponds to the mass transfer between solid and fluid phases, which is treated as a source term.

$$\frac{\partial}{\partial t}\iiint_{\mathcal{V}_f} c_f d\mathcal{V}_f + \iint_S c_f \mathbf{V}\cdot\mathbf{dS} = \iint_S J_{diff}\cdot\mathbf{n}\,\mathbf{dS} + \frac{\partial}{\partial t}\iiint_{\mathcal{V}_s} c_s d\mathcal{V}_s \tag{31}$$

Similarly to the continuity equation, in the limit as dz becomes very small

$$\frac{\partial}{\partial t}\iiint_{\mathcal{V}_f} c_f d\mathcal{V}_f = \frac{\partial}{\partial t}\left(c_f A_f dz\right) \tag{32}$$

$$\frac{\partial}{\partial t}\iiint_{\mathcal{V}_s} c_s d\mathcal{V}_s = \frac{\partial}{\partial t}\left(c_s A_s dz\right) \tag{33}$$

The surface integrals in the limit of dz become

$$\iint_S c_f \mathbf{V}\cdot\mathbf{dS} = c_f v dA_f + c_f A_f dv + v A_f dc_f \tag{34}$$

From the Divergence theorem in multi-variable calculus, we have

$$\iint_S J_{diff}\cdot\mathbf{n}\,\mathbf{dS} = \iiint_{\mathcal{V}_f} \nabla J_{diff} d\mathcal{V}_f = \nabla \iiint_{\mathcal{V}_f} J_{diff} d\mathcal{V}_f = \nabla\left(J_{diff} A_f dz\right)$$

(35)

By substituting the equations derived above into Equation 31 we obtain

$$\frac{\partial\left(c_f A_f\right)}{\partial t}+\frac{\partial\left(c_f A_f v\right)}{\partial z}=\frac{\partial\left(c_s A_s\right)}{\partial t}+\frac{\partial\left(J_{diff} A_f\right)}{\partial z} \tag{36}$$

By defining $A_f = A\cdot\phi$, $A_s = A\cdot(1-\phi)$ and $u = V\cdot\phi$, and assuming that A is constant, the above equation becomes

$$\frac{\partial\left(c_f\phi\right)}{\partial t}+\frac{\partial\left(c_f u\right)}{\partial z}=\frac{\partial\left(c_s(1-\phi)\right)}{\partial t}+\frac{\partial\left(J_{diff}\phi\right)}{\partial z} \tag{37}$$

By assuming that $\frac{\partial\phi}{\partial t}=0$ and expanding J_{diff}, we get

$$\frac{\partial c_f}{\partial t}+\frac{1}{\phi}\frac{\partial\left(c_f u\right)}{\partial z}=\frac{(1-\phi)}{\phi}\frac{\partial c_s}{\partial t}+\frac{1}{\phi}\frac{\partial}{\partial z}\left(D_e^M\frac{\partial c_f}{\partial z}\right) \tag{38}$$

The equation can be further simplified if $\frac{\partial u}{\partial z}=\frac{\partial\phi}{\partial z}=D_e^M=0$, which corresponds to the assumptions of constant velocity along the bed(which might be a case of isothermal and low-Mach number flow), constant porosity(which comes from the assumption of constant area for both solid and fluid phase) and no radial diffusion.

$$\frac{\partial c_f}{\partial t}+\frac{u}{\phi}\frac{\partial c_f}{\partial z}=\frac{1-\phi}{\phi}\frac{\partial c_s}{\partial t} \tag{39}$$

The Equation 39 is equivalent to the equation presented by Reverchon [6].

A.2. Thermodynamic

A.2.1. Equation of state and properties of the fluid phase

A cubic equation of state serves as a mathematical model to describe the behavior of real gases and liquids through a third-degree polynomial equation that correlates the pressure, volume, and temperature of a substance. These equations constitute tools for comprehending the phase behavior, properties, and thermodynamic processes of actual substances, across various engineering and scientific applications. The cubic equation of state take into account deviations from ideal gas behavior, which are particularly important at high pressures and low temperatures, where real gases do not follow assumption of ideal gas.

$$P=\frac{RT}{\upsilon_m-b}-\frac{\Phi}{\upsilon_m^2-ub\upsilon_m+wb^2} \tag{40}$$

In this equation, P denotes the pressure of the substance, υ_m represents the molar volume of the substance, T stands for the absolute temperature of the substance, u and w are integers that vary from one equation to another, R symbolizes the universal gas constant, and a and b serve as substance-specific parameters known as Van der Waals constants. ω denotes an acentric factor and $\Phi = a\alpha$.

The Van der Waals constants, a and b, constitute empirical values contingent upon the particular substance being modeled. These constants factor in molecular interactions (represented by 'a') and the finite size of gas molecules (indicated by 'b').

Several variations of the cubic equation of state exist each with its own set of parameters and assumptions. Tables 2 show parameters for popular cubic EoS.

EoS	u	w	a	b
van der Waals	0	0	$\frac{27}{64}\frac{R^2T_c^2}{P_c}$	$\frac{RT_c}{8P_c}$
Redlich and Kwong	1	0	$0.42748\frac{R^2T_c^{2.5}}{P_c}$	$\frac{0.08664RT_c}{P_c}$
Soave	1	0	$0.42748\frac{R^2T_c^2}{P_c}$	$\frac{0.08664RT_c}{P_c}$
Peng and Robinson [18]	2	-1	$0.45724\frac{R^2T_c^2}{P_c}$	$\frac{0.07780T_c}{P_c}$

Table 2: Parameters for Popular Cubic EoS

EoS	α	f(ω)
van der Waals	-	-
Redlich and Kwong	$\frac{1}{\sqrt{T_r}}$	-
Soave	$\left[1+f(\omega)\left(1-\sqrt{T_r}\right)\right]^2$	0.48+1.574ω-0.176ω^2
Peng and Robinson (Peng and Robinson [18])	$\left[1+f(\omega)\left(1-\sqrt{T_r}\right)\right]^2$	0.37464+1.54226ω-0.26992ω^2

Table 3: Parameters for Popular Cubic EoS

The general cubic equation of state can be represented as a polynomial, as indicated in Equation 41. In a one-phase region, the fluid is characterized by a single real root, corresponding to the gas, liquid, or supercritical phase. In the two-phase region, a gas-liquid mixture exists, and two roots are identified. The larger root corresponds to the gas phase, while the smaller root pertains to the liquid phase.

$$Z^3-(1+B-uB)Z^2+(A+wB^2-uB-uB^2)Z-AB-wB^2-wB^3=0 \tag{41}$$

where $A=\frac{\Phi P}{R^2T^2}$ and $B=\frac{bP}{RT}$.

If the Peng-Robinson equation of state (Peng and Robinson [18]) is used, the polynomial equation becomes

$$Z^3-(1-B)Z^2+(A-2B-3B^2)Z-(AB-B^2-B^3)=0 \tag{42}$$

For an ideal gas, the compressibility factor is defined as $Z=1$, but to describe real-life physical phenomena, the deviation of Z needs to be consider. The value of Z typically increases with pressure and decreases with temperature. At elevated pressures, molecules collide more frequently, allowing repulsive forces between molecules to influence the molar volume of the real gas (υ_m) to surpass that of the corresponding ideal gas $\left(\left(\upsilon_m\right)_{ideal\ gas}=\frac{RT}{P}\right)$, resulting in Z exceeding one. At lower pressures, molecules move freely, with attractive forces predominating, leading to $Z<1$.

Numerical methods such as Newton-Raphson can be used to solve the polynomial equation to obtain the compressibility $Z\left(T(t,z),P(t)\right)$ at given temperature and pressure. Alternatively, the closed form solution can by obtained by Cardano formula. Details regarding the Cardano formula can be found in Appendix A.3.

A.2.2. Density of the fluid phase

The density of the fluid can be calculated from the real gas equation $\rho=\frac{P}{RTZ}\frac{1}{m_{CO2}}$. The local temperature can be obtain from the time evolution of governing equations, the pressure is consider to be constant along the system to be a know at any time. The local compressibility factor can be also computed if the local temperature and pressure are know. To obtain the density in terms of mass, molar mass of the solvent is taken into account.

A.3. Cardano's Formula

Following the work of Gmehling et al. [19], a cubic equation of state can be written a following form

$$Z^3 + UZ^2 + SZ + T = 0 \tag{43}$$

with Z as the compressibility factor. Using Cardano's formula, this type of equation can be solved analytically. With the abbreviations

$$P = \frac{3S - U^2}{3} \qquad Q = \frac{2U^3}{27} - \frac{US}{3} + T$$

the discriminant can be determined to be

$$D = \left(\frac{P}{3}\right)^3 + \left(\frac{Q}{2}\right)^2 \tag{44}$$

For $D > 0$, the equation of state has one real solution:

$$Z = \left[\sqrt{D} - \frac{Q}{2}\right]^{1/3} - \frac{P}{3\left[\sqrt{D} - \frac{Q}{2}\right]^{1/3}} - \frac{U}{3} \tag{45}$$

For $D < 0$, there are three real solutions. With the abbreviations

$$\Theta = \sqrt{-\frac{P^3}{27}} \qquad \Phi = \arccos\left(\frac{-Q}{2\Theta}\right)$$

they can be written as

$$Z_1 = 2\Theta^(1/3)\cos\left(\frac{\Phi}{3}\right) - \frac{U}{3} \tag{46}$$

$$Z_2 = 2\Theta^(1/3)\cos\left(\frac{\Phi}{3} + \frac{2\pi}{3}\right) - \frac{U}{3} \tag{47}$$

$$Z_3 = 2\Theta^(1/3)\cos\left(\frac{\Phi}{3} + \frac{4\pi}{3}\right) - \frac{U}{3} \tag{48}$$

The largest and the smallest of the three values correspond to the vapor and to the liquid solutions, respectively. The middle one has no physical meaning.

A.4. Maximum likelihood

Maximum likelihood estimation (MLE) is a statistical method used to estimate the parameters of a probability distribution based on observed data. The MLE works by finding the values of the parameters that maximize the likelihood function, which is the probability of observing the given data for a given set of parameter values. The MLE has desirable properties such as asymptotic efficiency and normality. Although the MLE has often been associated with the normal distribution for mathematical convenience, it can be applied to a wide range of probability distributions.

To find the maximum likelihood estimates, we maximize the joint probability density function, or likelihood function, denoted as $p(\theta|y(t_1), y(t_2), ..., y(t_n))$, where θ represents the parameters and $y(t_1), y(t_2), ..., y(t_n)$ represent the observed data. The conditions at the maximum can be refined by incorporating prior information. The posterior probability density function $p(\theta|y)$ can be expressed as the ratio of two probability densities using the continuous variable analogue of Bayes' theorem . In such a case the posteriori distribution is given by Equation 49.

$$p\left(\theta|y(t_n), ..., y(t_1)\right) = \frac{p\left(\theta, y(t_n), ..., y(t_1)\right)}{p\left(y(t_n), ..., y(t_1)\right)} \tag{49}$$

The numerator of the right-hand side od Equation 49 becomes

$$\begin{aligned} p\left(\theta, y(t_n), ..., y(t_1)\right) &= p\left(y(t_n)|\theta, y(t_{n-1}), ..., y(t_1)\right) \\ &\cdot p\left(\theta, y(t_{n-1}), ..., y(t_1)\right) \end{aligned} \tag{50}$$

These operations can be continued repetitively until we get

$$p\left(\theta, y(t_n), ..., y(t_1)\right) = p(\theta)\prod_{i=1}^{n} p\left(y(t_i)|\theta, y(t_{i-1}), ..., y(t_1)\right) \tag{51}$$

Examination of Equation 19 shows that $dY(t_i)/dt$ depends only on t_i, θ and $\epsilon(t_i)$ and is not conditioned by any previous measurement. Consequently, we can write

$$p\left(y(t_i)|\theta, y(t_{i-1}), ..., y(t_1)\right) = p\left(y(t_i)|\theta\right) \tag{52}$$

provided Equation 19 is observed as a constraint. The desired joint conditional probability function is thus

$$p\left(\theta|y(t_n), ..., y(t_1)\right) = \frac{p(\theta)\prod_{i=1}^{n} p\left(y(t_i)|\theta\right)}{p\left(y(t_n), ..., y(t_1)\right)} \tag{53}$$

We can get rid of the evidence term $p\left(y(t_n), ..., y(t_1)\right)$ because it's constant with respect to the maximization. Moreover, if we are lacking a prior distribution over the quantity we want to estimate, then $p(\theta)$ can be omitted. In such a case:

$$p\left(\theta|y(t_n), ..., y(t_1)\right) = \prod_{i=1}^{n} p\left(y(t_i)|\theta\right) = \prod_{i=1}^{n} L\left(\theta|y(t_i)\right) \tag{54}$$

The likelihood function $L(\theta|y)$ for the parameters based on several observations is the product of the individual functions if the observations are independent.

$$\begin{aligned} L\left(\theta|y(t_n), ..., y(t_1)\right) &= \prod_{i=1}^{n} L\left(\theta|y(t_i)\right) \\ &= p\left(y(t_1)|\theta\right) p\left(y(t_2)|\theta\right) ... p\left(y(t_n)|\theta\right) \end{aligned} \tag{55}$$

In choosing as estimates of θ the values that maximize L for the given values $\left(y(t_i)\right)$, it turns out that it is more convenient to work with the $\ln L$ than with L itself:

$$\ln L = \ln p\left(y(t_1)|\theta\right) + \ln p\left(y(t_2)|\theta\right) + ... + \ln p\left(y(t_n)|\theta\right) = \sum_{i=1}^{n} \ln p\left(y(t_i); \theta\right) \tag{56}$$

By assuming that the conditional distribution of $\bar{Y}_i$, given y_i, is normal, then we form the likelihood function based on the probability density:

$$\begin{aligned} p\left(\theta, \sigma|y(t_n), ..., y(t_1)\right) &= \prod_{i=1}^{n} \frac{1}{\sqrt{2\pi}\sigma} \exp\left[\frac{1}{2\sigma}\left(Y(t_i) - y(\theta, t_i)\right)^2\right] \\ L\left(\theta, \sigma|y(t_n), ..., y(t_1)\right) &= \prod_{i=1}^{n} \frac{1}{\sqrt{2\pi}\sigma} \exp\left[\frac{1}{2\sigma}\left(Y(t_i) - y(\theta, t_i)\right)^2\right] \end{aligned} \tag{57}$$

where σ is the variance

By taking the natural logarithm of the Equation 57, the final form of the objective function can be obtained:

$$\ln L = -\frac{n}{2}\left(\ln(2\pi) + \ln\sigma^2\right) - \frac{\sum_{i=1}^{n}\left[Y(t_i) - y(\theta, t_i)\right]^2}{2\sigma^2} \tag{58}$$